Available online at www.sciencedirect.com
SCIENCE DIRECT®
ELSEVIER
International Journal of Mass Spectrometry 228 (2003) 541–549
International Journal of Mass Spectrometry
www.elsevier.com/locate/ijms

Electron attachment and detachment: cyclo-$C_4F_4Cl_2$

Jane M. Van Doren[a], Sarah A. McSweeney[a], Matthew D. Hargus[a], Donna M. Kerr[a], Thomas M. Miller[b,*], Susan T. Arnold[b], A.A. Viggiano[b]

[a] *Department of Chemistry, College of the Holy Cross, Worcester, MA 01610-2395, USA*
[b] *Air Force Research Laboratory, Space Vehicles Directorate, Hanscom Air Force Base, 29 Randolph Road VSBXT, Bedford, MA 01731-3010, USA*

Received 14 December 2002; accepted 19 March 2003

Abstract

Electron attachment to 1,2-dichlorotetrafluorocyclobutene (c-$C_4F_4Cl_2$) and electron detachment from the parent anion (c-$C_4F_4Cl_2^-$) have been studied over a temperature range from 295 to 556 K in a flowing-afterglow Langmuir-probe (FALP) apparatus. Electron attachment to c-$C_4F_4Cl_2$ over this temperature range yields only the parent anion in a helium buffer gas at 80–160 Pa pressure. The electron attachment rate constant was found to be independent of temperature over the range studied, at a value of $(2.4 \pm 0.8) \times 10^{-7}$ cm^3 s^{-1}, that is, essentially upon every collision. The rate constant for electron detachment from c-$C_4F_4Cl_2^-$ is strongly temperature dependent, being imperceptible at room temperature and climbing to a value of 3100 ± 1200 s^{-1} at 511 K. The equilibrium constant obtained from these data yields the electron affinity (EA) of c-$C_4F_4Cl_2$ of 0.87 ± 0.08 eV. G3(MP2) and density functional theory (DFT) calculations were carried out for the $C_4F_4Cl_2$ neutral, anion, and fragments in order to aid in interpreting the experiments. Both the G3(MP2) and DFT calculations yield values for EA(c-$C_4F_4Cl_2$), 0.79 and 0.93 eV, respectively, that are in good agreement with the experimental value. The calculations also show that there are no open exothermic dissociative electron attachment channels for c-$C_4F_4Cl_2$. Further, we present structures, atomic charges, dipole moments, heat capacities, and polarizabilities for these molecules. The results are contrasted with previous results on 1,2-dichlorooctafluorocyclohexene (c-$C_6F_8Cl_2$) and 1,2-dichlorohexafluorocyclopentene (c-$C_5F_6Cl_2$), both of which possess larger EAs.

Keywords: Electron attachment; Electron affinity; $C_4F_4Cl_2$ (1,2-dichlorotetrafluorocyclobutene); Flowing-afterglow Langmuir-probe; Kinetics; G3(MP2); Density functional theory

1. Introduction

Several years ago we published the results of experiments [1] and calculations [2] on the competition between nondissociative and dissociative electron attachment to 1,2-dichlorooctafluorocyclohexene (c-$C_6F_8Cl_2$) and 1,2-dichlorohexafluorocyclopentene (c-$C_5F_6Cl_2$). For those molecules, the parent anion was the only product of electron attachment at room temperature. As the temperature was increased, Cl^- product appeared, and in the range 520–540 K, Cl^- became the dominant product of attachment. At the time our computational capabilities limited us to density functional methods for molecules of the size of c-$C_6F_8Cl_2$ and c-$C_5F_6Cl_2$. Although only accurate to about 0.3 eV, these calculations were adequate to explain the experimental results. The calculations

* Corresponding author. Tel.: +1-781-3775031; fax: +1-781-3777091.
E-mail address: thomas.miller@hanscom.af.mil (T.M. Miller).

1387-3806/$ – see front matter © 2003 Elsevier Science B.V. All rights reserved.
doi:10.1016/S1387-3806(03)00161-1

yielded electron affinities (EAs): EA(c-$C_6F_8Cl_2$) = 1.46 eV and EA(c-$C_5F_6Cl_2$) = 1.17 eV and gave dissociative attachment endothermicities consistent with the observations of the increase in the Cl^- product with temperature.

The present case of 1,2-dichlorotetrafluorocyclobutene (c-$C_4F_4Cl_2$) is different. Calculations indicate that production of Cl^- ion product in electron attachment is endothermic by enough that dissociative electron attachment is unlikely to be observed in our temperature range, so there is no competition between nondissociative and dissociative attachment. On the other hand, EA(c-$C_4F_4Cl_2$) is calculated to be low enough that thermal electron detachment may be observed at our highest temperatures. In this article we report experiments on electron attachment to c-$C_4F_4Cl_2$ and thermal electron detachment from c-$C_4F_4Cl_2^-$, as well as density functional and more accurate G3(MP2) calculations on the parent neutral and anion and fragments.

2. Experiment

A flowing-afterglow Langmuir-probe (FALP) apparatus was used in the present work. The FALP method and this particular apparatus at the Air Force Research Laboratory have been described previously [3,4]. A diffusion-dominated electron/positive-ion plasma was established in fast-flowing He gas in a 1-m long flow tube of 7.8-cm diameter. The He buffer gas pressure could be varied from 80 to 160 Pa, but was 133 Pa for most of the experiments reported here. A partial pressure of ~3 Pa Ar gas was added upstream of the c-$C_4F_4Cl_2$ inlet port to remove metastable-excited He by Penning ionization and He_2^+ by charge transfer, so that the plasma consisted of electrons, He^+, and Ar^+ as it reached the position of the c-$C_4F_4Cl_2$ inlet port. With no c-$C_4F_4Cl_2$ present, the ambipolar-diffusion decay rate of the electron density along the axis of the flow tube was measured using a movable Langmuir-probe. With c-$C_4F_4Cl_2$ added through the inlet port, the decay rate of the electron density along the flow tube axis initially greatly increased due to electron attachment, but at longer times reached a steady-state condition as a result of a balance between electron attachment to c-$C_4F_4Cl_2$ and thermal electron detachment from c-$C_4F_4Cl_2^-$. By fitting the decay rate to a solution of the differential equations describing the coupled effects of diffusion, attachment, and detachment, we obtained both the electron attachment rate constant k_a and the detachment rate constant k_d, as described in our earlier work [5,6]. Both rate constants may be determined from one data set because the attachment rate constant dominates behavior at short reaction times, while the ratio of k_d to k_a dominates behavior at long times. The time scale was determined by using the Langmuir-probe to measure the propagation speed of a pulse disturbance in the electron density along the axis of the flow tube. A sample of the data is presented in Fig. 1 for a He pressure of 133 Pa at 490 K and a c-$C_4F_4Cl_2$ concentration of $n_r = 6.0 \times 10^9\,cm^{-3}$. The upper curve in this figure, without c-$C_4F_4Cl_2$ present, gives an ambipolar-diffusion decay constant $\nu_D = 543\,s^{-1}$. The middle curve is a fit to the data obtained with c-$C_4F_4Cl_2$ present, and yielded k_a =

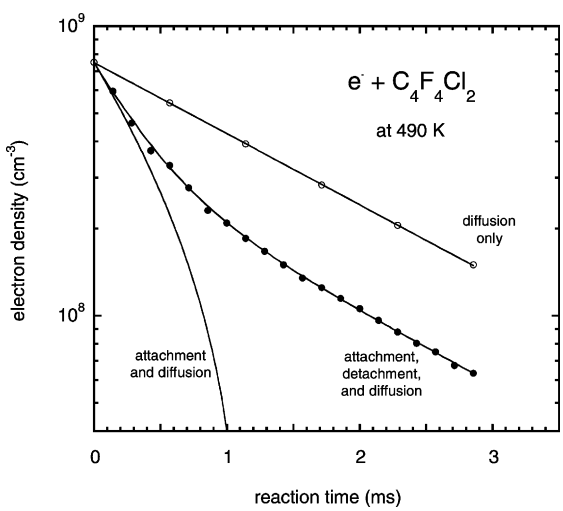

Fig. 1. Electron density decay along the flow tube axis, showing the approach to a steady-state, diffusion-limited condition at long times. The line passing through the solid points is a fit to the data of a solution to the rate equation governing free electron density loss due to attachment and diffusion, and electron density gain due to thermal detachment.

$2.3 \times 10^{-7}\,cm^3\,s^{-1}$ and $k_d = 1480\,s^{-1}$. The lower curve shows what to expect if there were no electron detachment. As described in [5], this situation is ideal for determining k_a and k_d because the attachment frequency, $\nu_a = k_a n_r = 1380\,s^{-1}$ is comparable to the detachment rate k_d, and both are larger than the diffusion decay constant. If either k_a or k_d dominates, the other is determined with less precision. If ν_D is large, the plasma diffuses away before reaching the steady-state condition illustrated in Fig. 1.

Determinations of k_a and k_d are only dependent on relative measurements of the electron density. Absolute knowledge of the initial electron density $n_e(0)$ is needed to assure first-order kinetics, i.e., $n_r \gg n_e(0)$, and to ensure that loss of electron density to electron–ion recombination is negligible [7]. The uncertainties in the experiment are associated with (a) relative measurements of the electron density along the flow tube axis, (b) measurements of the flow tube pressure and of flow rates of the buffer and reactant gases, using commercial pressure gauges and flow controllers (MKS, Inc., Andover, MA), and (c) in fitting the data to obtain both k_a and k_d. We estimate that k_a is accurate to within ±35%, and with a precision (relative accuracy) of ±10%. The apparent k_d may be determined with similar accuracy when the attachment frequency is comparable to the detachment frequency, but there are indications (discussed below) that additional uncertainty is incurred because the He gas is inefficient at thermalizing the negative ions formed in attachment. We estimate that the k_d are accurate within ±40% in the temperature range 490–511 K, where k_a and k_d are comparable. In any case, EA(c-$C_4F_4Cl_2$) may still be determined rather accurately from k_a and k_d as outlined in [5], because EA(c-$C_4F_4Cl_2$) is only logarithmically dependent on the equilibrium constant k_a/k_d.

An rf quadrupole mass spectrometer sampled ions through an aperture at the terminus of the flow tube in order to determine the ion product of electron attachment (only c-$C_4F_4Cl_2^-$ in this case).

The c-$C_4F_4Cl_2$ was purchased from Lancaster Synthesis, Inc. (Windham, NH) and used without further purification except for degassing with several freeze–pump–thaw cycles. Because a very small concentration of c-$C_4F_4Cl_2$ is needed in the flow tube (ca. 0.3 ppm by volume), a dilute mixture (∼0.2%) of c-$C_4F_4Cl_2$ in He gas was prepared in a 1-L passivated stainless steel bulb for titration into the flow tube. Reactant gas entered the flow tube through a port consisting of three hollow needles that protruded radially into the flow tube at a point about halfway down its length.

3. Calculations

Density functional theory (DFT) has been used here to determine the energetics related to nondissociative and dissociative electron attachment to c-$C_4F_4Cl_2$. Becke's three-parameter functional B3PW91 [8] was used with the 6-311+G(3df) basis set to compute total energies of the parent neutral and anion, and of dissociation fragments, at 0 and 298 K. From these total energies, the EA, bond enthalpies, and dissociative electron attachment reaction enthalpy were determined. Comparison is made with calculations of the same quantities using the more accurate G3(MP2) method [9].

Calculations of the total energies of the c-$C_4F_4Cl_2$ parent molecule and fragments were carried out using the GAUSSIAN-98W program package [10]. The DFT techniques are the same as those described in our paper on c-$C_5F_6Cl_2$ and c-$C_6F_8Cl_2$ [2]. Becke's B3PW91 functional [8] includes the Perdew et al. non-local correlation functional [11]. The B3PW91 functional is one of several that others have found to yield electron affinities of acceptable accuracy (see the review of Rienstra-Kiracofe et al. [12]). It was used in the present work for direct comparison with our earlier results for larger halogenated cyclic alkenes.

For the DFT method as applied to the present problem, the parent and fragment molecules were first geometry-optimized using the B3PW91/6-311+G(d) functional and basis set with tight convergence of self-consistent field (SCF) integrals, and a harmonic frequency analysis was performed at the same level of theory to give the zero-point energies (ZPEs) and thermal corrections to energies at 298.15 K and 1 atm

Table 1
Total energies and ZPE for c-$C_4F_4Cl_2$ and dissociation fragments, all in hartree units

Molecule	Method	ZPE[a]	Total energy[b] (0 K)	Enthalpy[c] (298 K)
c-$C_4F_4Cl_2$ (C_{2v} point group, $^1A_1$)	DFT	0.03565	−1472.04514	−1472.03502
	G3(MP2)	0.03718	−1470.66578	−1470.65579
c-$C_4F_4Cl_2^-$ (C_2 point group, ^2A)	DFT	0.03222	−1472.07936	−1472.06862
	G3(MP2)	0.03400	−1470.69488	−1470.68446
c-C_4F_4Cl (C_s point group, $^2A'$)	DFT	0.03243	−1011.77565	−1011.76680
	G3(MP2)	0.03360	−1010.81515	−1010.80652
c-$C_4F_4Cl^-$ (C_s point group, $^1A'$)	DFT	0.03105	−1011.88936	−1011.88047
	G3(MP2)	0.03255	−1010.93632	−1010.92756
Cl	DFT	0	−460.11130	−460.10891
	G3(MP2)	0	−459.68724	−459.68488
Cl^-	DFT	0	−460.24517	−460.24281
	G3(MP2)	0	−459.82236	−459.82000
e^-	5*kT*/2	0	0	+0.00236

[a] For DFT, B3PW91/6-311+G(d) level of theory, and scaled by 0.9316; for G3(MP2), HF/6-31G(d) level of theory, scaled by 0.9316.
[b] For DFT, B3PW91/6-311+(3df)//B3PW91/6-311+G(d) plus ZPE; for G3(MP2), an approximation to QCISD(T)/6-311+G(3d)//MP2(Full)/6-31G(d) plus ZPE (see text).
[c] Energy at 0 K with a 0–298 K enthalpy correction calculated at the level of theory as given in footnote a, with scaled vibrational frequencies.

pressure. The vibrational frequencies were scaled by the empirical factor 0.9613 in calculating both the ZPE and thermal corrections [13]. The thermal correction for the electron and Cl^- is 5*kT*/2, and that for Cl is slightly greater because of spin-orbit splitting [14]. Stability of all wavefunctions was checked, i.e., we verified that the molecular orbital set chosen gave the lowest energy wavefunctions in each case. Next, single-point energies were calculated using the 6-311+G(3df) basis set and tight convergence of SCF integrals. ZPE and thermal energy corrections were then applied to the total energies; all these quantities are given in Table 1.

More accurate G3(MP2) theory [9] was also applied to this problem using the same program package [10]. G3(MP2) theory is a simplification of the G3 method with basis set extension corrections made at the MP2 level. In this method, QCISD(T) calculations are carried out with a modest basis set [6-31G(d)]. MP2 calculations are carried out with this and a larger basis set [6-311+G(3df)], and used to correct the QCISD(T) results to the larger basis set. ZPE and thermal corrections are calculated at the HF/6-31G(d) level of theory (including geometry-optimization), with vibrational frequencies scaled by the empirical factor 0.8929 [7]. The stability of the wavefunctions was verified. The molecular geometries were then optimized at the MP2(Full)/6-31G(d) level, prior to performing the single-point energy calculations outlined before. These more accurate calculations were not feasible in our earlier work with larger molecules (c-$C_5F_6Cl_2$ and c-$C_6F_8Cl_2$) [2]. The comparison here between DFT and G3(MP2) results for c-$C_4F_4Cl_2$ gives us confidence that the uncertainty (±0.3 eV) which we estimated for the DFT results is reasonable.

Derived quantities are given in Table 2. The adiabatic EA was calculated from the difference in 0 K total energies of parent molecules and respective anions. Bond enthalpies were calculated from differences in total energies of parent molecule and the sum of fragment energies. The reaction enthalpy for dissociative electron attachment (yielding Cl^- product ion and C_4F_4Cl radical ring fragment) was calculated from differences in the total energies given in Table 1.

Tests of DFT by others have shown that thermochemical quantities such as atomization energies,

Table 2
Adiabatic EA, bond enthalpies (D), and dissociative attachment reaction enthalpy (ΔH_{rxn}) for production of Cl^-, all in eV, calculated from the energies given in Table 1

Quantity	Method	Energy (0 K)	Enthalpy (298 K)
EA(c-$C_4F_4Cl_2$)	DFT	0.93	–
	G3(MP2)	0.79	–
D(c-C_4F_4Cl–Cl)	DFT	4.30	4.34
	G3(MP2)	4.45	4.47
D(c-C_4F_4Cl–Cl^-)	DFT	1.59	1.61
	G3(MP2)	1.56	1.58
EA(c-C_4F_4Cl)	DFT	3.09	–
	G3(MP2)	3.30	–
$\Delta H_{rxn}(Cl^-)$	DFT	+0.66	+0.63
	G3(MP2)	+0.77	+0.73

ionization potentials, and proton affinities using the B3LYP/6-311++G(3df,2p) functional and basis set (the "2p" and second "+" apply to hydrogen atoms, which we do not have in the present work) are good on average to ±0.13 eV but with worst-case errors of about 0.5 eV [15]. The G3(MP2) method has been found by Curtiss et al. [9] to give various energy differences such as EAs within 56 meV, on average.

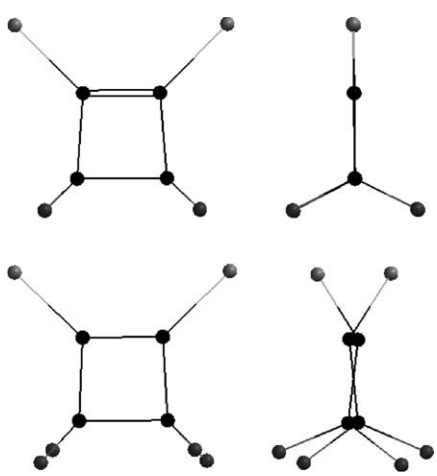

Fig. 2. Optimized geometries from B3PW91/6-311+G(d) calculations; views above and to one side of the rings. Top: c-$C_4F_4Cl_2$. Bottom: c-$C_4F_4Cl_2{}^-$. The two Cl atoms are at the top of each sketch, bound to C1 and C2. The other C atoms in the rings each have two F atoms bound to them.

Table 3
A sampling of bond lengths (Å) and angles (°), with geometries optimized at the B3PW91/6-311+G(d) and MP2(Full)/6-31G(d) levels of theory

Bond length or angle	c-$C_4F_4Cl_2$		c-$C_4F_4Cl_2{}^-$	
	B3PW91	MP2(Full)	B3PW91	MP2(Full)
C1–C2	1.345	1.352	1.417	1.428
C2–C3	1.506	1.502	1.476	1.474
C1–C4	1.506	1.502	1.476	1.474
C3–C4	1.570	1.552	1.552	1.534
C1–Cl1	1.688	1.685	1.784	1.771
C2–Cl2	1.688	1.685	1.784	1.771
C1C2C3	94.3	93.8	91.9	90.9
C2C1C4	94.3	93.8	91.9	90.9
C2C3C4	85.7	86.2	86.7	86.8
C1C4C3	85.7	86.2	86.7	86.8
C2C1Cl1	134.6	134.9	127.0	126.5
C1C2Cl2	134.6	134.9	127.0	126.5
Dihedral[a]	0	0	72.3	75.0
Dihedral[b]	0	0	−12.0	−15.6

[a] The angle between the chlorine atoms looking along the C1–C2 bond.
[b] The angle between the C1 and C2 atoms looking along the C3–C4 bond (a measure of the twisting of the ring).

Relevant to the present comparison with the DFT results, EA(Cl) is found to be 3.677 eV using the G3(MP2) prescription, which is in agreement with the experimental value of 3.612724 ± 0.000027 eV

Table 4
Natural population analysis of charges from electron densities calculated at the B3PW91/6-311+G(3df) level of theory (geometries optimized at the B3PW91/6-311+G(d) level)

Atom	c-$C_4F_4Cl_2$	c-$C_4F_4Cl_2{}^-$	Difference
C1	−0.123	−0.253	−0.130
C2	−0.123	−0.253	−0.130
C3	+0.696	+0.645	−0.051
C4	+0.696	+0.645	−0.051
Cl1	+0.120	−0.111	−0.231
Cl2	+0.120	−0.111	−0.231
F31	−0.346	−0.390	−0.044
F32	−0.346	−0.391	−0.045
F41	−0.346	−0.390	−0.044
F42	−0.346	−0.391	−0.045

F31 and F32 in the table denote the two F atoms bonded to C3, etc.

Table 5
Heat capacities (C_p) and average polarizabilities (α) calculated using B3PW91/6-311+G(d) functional and basis set

Molecule	C_p (cal mol^{-1} K^{-1})	μ_d (D)	α (Å^3)
c-$C_4F_4Cl_2$ ($^1A_1$)	33.3	2.14	10.4
c-$C_4F_4Cl_2^-$ (^2A)	35.0	–	13.2
c-C_4F_4Cl ($^2A'$)	29.2	1.80	8.5
c-$C_4F_4Cl^-$ ($^1A'$)	29.8	–	10.4

The dipole moments (μ_d) are from a higher level B3PW91/6-311+G(3df) calculation based on the B3PW91/6-311+G(d) geometry.

[16]. Also, EA(Cl_2) = 2.481 eV is found using the G3(MP2) method, close to the experimental value of 2.38 ± 0.01 eV [12]. It may be seen from the energies calculated in Table 1 that DFT performs well compared to G3(MP2); the largest discrepancy is 0.21 eV.

It is interesting to compare the results in Table 2 to analogous quantities calculated for c-$C_5F_6Cl_2$ and c-$C_6F_8Cl_2$ in our earlier paper [2]. The bond dissociation energies for removing Cl from the parent neutral are essentially the same in all three molecules (ca. 4.1 eV), as are those for removing Cl^- from the parent anion (ca. 1.6 eV). In contrast, the EA of the molecule increases with ring size. This trend is presumably due to increased inductive stabilization afforded by the additional fluorine atoms. As observed for c-$C_5F_6Cl_2$ and c-$C_6F_8Cl_2$, the C–C double bond (C1–C2) and the allied C–Cl bonds in c-$C_4F_4Cl_2$ lengthen significantly upon attachment of the electron. Bond lengths and charges for the rest of the molecule are less affected. The optimized geometry of the anion indicates that the C1–C2 bond order is reduced and the ring structure remains intact. Fig. 2 shows views of the c-$C_4F_4Cl_2$ neutral and anion structures. Some relevant bond lengths and angles for c-$C_4F_4Cl_2$ are given in Table 3. Table 4 gives the electronic charge associated with each atom of the neutral and anion. Seventy-two percent of the attached electron ends up symmetrically on C1, C2, and their chlorine partners, and the other 28% has been partitioned to all other atoms in small pieces. Heat capacities, dipole moments, and polarizabilities are given in Table 5. In the present case, for c-$C_4F_4Cl_2$, Fig. 2 (and Table 3) shows that there is a 12–16° twist induced in the ring by electron attachment.

4. Results and discussion

Electron attachment to c-$C_4F_4Cl_2$ was found to produce only the parent anion in the temperature range 295–556 K. The experimental results are given in Table 6. It is seen that the electron attachment rate constant for c-$C_4F_4Cl_2$ is independent of temperature, at an average value of (2.4 ± 0.8) × 10^{-7} cm^3 s^{-1}, over the range 295–556 K. This rate constant is close to collisional in magnitude. Using the calculated polarizability (Table 5) with the capture theory of Klots [17], a collisional rate constant of 3.3 × 10^{-7} cm^3 s^{-1} is predicted at 295 K, declining by 17% as the temperature is increased to 556 K. (The dipole moment is thought not to affect the rate constant by more than a few percent [18].) The thermal electron detachment rate constant is undetectable at room temperature, but becomes measurable in the 450–500 K temperature range, and is 3100 ± 1200 s^{-1} at 511 K. It is difficult to fit data at temperatures much above 511 K because the detachment rate becomes so large that the steady-state condition illustrated in Fig. 1 is reached at shorter reaction times, leaving precious little data to fit with two parameters. The data obtained at 556 K suffer from this problem, and we can only place a lower limit on the detachment rate constant, as given in Table 6.

Fig. 3 shows k_d plotted vs. 1/kT. Thermal electron detachment is not an Arrhenius process, but the exponential 1/T dependence dominates the behavior of

Table 6
Rate constants (k_a) for electron attachment to c-$C_4F_4Cl_2$ and rate constants (k_d) for thermal electron detachment from c-$C_4F_4Cl_2^-$, as a function of temperature

T (K)	k_a (10^{-7} cm^3 s^{-1})	k_d (s^{-1})
295	2.4	0
366	2.6	0
456	2.3	850
490	2.3	1480
496	2.5	2550
508	2.4	2950
511	2.6	3100
556	2.5	>7200

The k_a are estimated accurate within ±35%, and the k_d at 490–511 K are estimated accurate within ±40%.

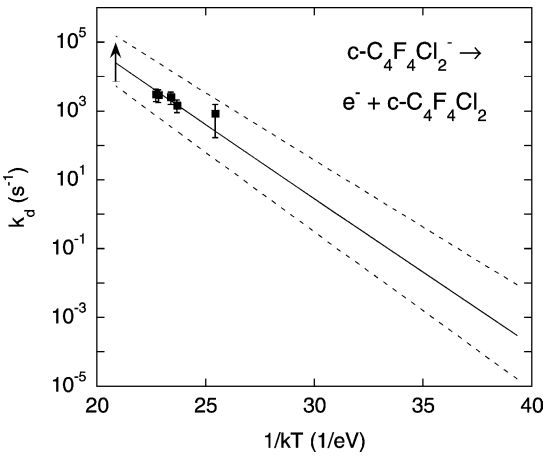

Fig. 3. Thermal electron detachment rate constants determined in the present work (solid squares and a lower limit indicated by an arrow). The lines are k_d predicted by Eq. (1) using the measured k_a and EA(c-$C_4F_4Cl_2$) = 0.87 ± 0.08 eV determined from the attachment/detachment equilibrium: the central line corresponds to 0.87 eV, the upper line is based on the lower bound to the EA (0.79 eV), and the lower line is based on the upper bound to the EA (0.95 eV).

k_d with T provided that k_a has a weak T dependence. Straightforward thermodynamics [5] for the attachment/detachment equilibrium yields.

$$k_d = k_a L_0 \left(\frac{273.15}{T}\right) \times \exp\left[\frac{-\mathrm{EA} - \Delta S - (H_T - H_0)}{kT}\right]. \quad (1)$$

The electron part of the entropy term ΔS in the argument of the exponential contributes a factor of $T^{5/2}$ to k_d, so the leading temperature dependence in Eq. (1) becomes $T^{3/2}$. In Eq. (1), k is Boltzmann's constant, L_0 is Loschmidt's number, EA is the electron affinity of c-$C_4F_4Cl_2$ (at 0 K, by definition), ΔS is the entropy change due to electron attachment, and $H_T - H_0$ is the thermal energy correction needed to reduce the EA result to 0 K. The entropy change is:

$$\Delta S = S(\text{anion}) - S(\text{neutral}) - S(\text{electron}). \quad (2)$$

The first two terms in Eq. (2) are nearly the same except for the electron spin degeneracy (the neutral is a singlet while the anion is a doublet) since the structures of the anion and neutral are similar. We may obtain these entropies from the DFT calculations described in the previous section. The DFT calculations yield $S(\text{anion}) - S(\text{neutral}) = 0.268\,\text{meV K}^{-1}$ at 490 K. The final term in Eq. (1) may be obtained from the JANAF tables [14] or evaluated as in [5]: $S(\text{electron}) = 0.325\,\text{meV K}^{-1}$ at 490 K, for example. The net entropy change at 490 K is $\Delta S = -0.057\,\text{meV K}^{-1}$. Now for the thermal correction to the EA:

$$H_T - H_0 = \int_0^T C_p(\text{anion})\,dT - \int_0^T C_p(\text{neutral})\,dT - \int_0^T C_p(\text{electron})\,dT. \quad (3)$$

The first two terms in Eq. (3) will essentially cancel if the geometries of the anion and neutral molecules are very nearly the same. We used the DFT method to obtain (at 490 K, for example) 582 meV for the anion term and 551 meV for the neutral-molecule term. That for the electron is $5kT/2 = 106$ meV. The net thermal correction is −75 meV.

The lines in Fig. 3 were generated from Eq. (1) using the (average) measured electron attachment rate constant $k_a = 2.4 \times 10^{-7}\,\text{cm}^3\,\text{s}^{-1}$ and three values of EA(c-$C_4F_4Cl_2$): the best-fit line (in the 490–511 K temperature range) corresponds to EA(c-$C_4F_4Cl_2$) = 0.87 eV. The dashed lines correspond to the upper and lower limits of the estimated uncertainty (±0.08 eV) in EA(c-$C_4F_4Cl_2$). Fig. 3 serves to show (a) how rapidly k_d changes with T, (b) in particular, how low k_d is at room temperature, (c) that the rate of change in k_d increases as EA increases, (d) that k_d may be determined in the FALP only over a very small T range (50 K at best), and (e) that EA(c-$C_4F_4Cl_2$) is rather insensitive to errors in k_d (because of the logarithmic dependence on the equilibrium constant k_a/k_d). No other experimental value for EA(c-$C_4F_4Cl_2$) exists for comparison.

Experiments at Montana State University [19] using azulene as the attaching gas over a wide pressure range imply that higher buffer gas pressures are required to achieve complete thermal equilibrium in electron attachment/detachment experiments. It is not possible to test the pressure dependence appreciably

using the FALP apparatus, for reasons detailed in a recent work [6]. An independent approach—with an ion-equilibration period, and not involving a plasma—was employed to corroborate the FALP detachment results. A selected ion flow tube (SIFT) apparatus [20] was adapted for this purpose [21]. Here, c-$C_4F_4Cl_2^-$ ions were prepared in the SIFT ion source and injected into a fast flow of He gas at 53 Pa pressure at temperatures in the range 300–550 K. SF_6 gas was added to the flow tube to scavenge electrons thermally detached from the equilibrated c-$C_4F_4Cl_2^-$ ions. The ratio between the resulting SF_6^- and surviving c-$C_4F_4Cl_2^-$ ion signals is determined by a detachment rate constant. While some uncertainties exist, the SIFT work gives us confidence that any error is covered by the ±40% error limits estimated for the FALP-derived k_d.

The computational results given in Table 2 augment the experimental ones in that (a) both the G3(MP2) and DFT values for EA(c-$C_4F_4Cl_2$), 0.79 and 0.93 eV, respectively, are in good agreement with the experimental one obtained from analysis of the attachment/detachment steady-state, 0.87 ± 0.08 eV; (b) production of Cl^- ion product in electron attachment to c-$C_4F_4Cl_2$ is too endothermic (0.7 eV) for a bimolecular process to occur in our temperature range, and indeed no Cl^- ion product was observed; (c) no c-$C_4F_4Cl^-$ ion product is expected in the temperature range of the present experiment, and none was observed, as dissociative attachment was calculated to be much too endothermic (1.2 eV); and (d) the bond enthalpies D_{298}(c-C_4F_4Cl–Cl) and D_{298}(c-C_4F_4Cl–Cl^-) are large enough that thermal dissociation of the reactant neutral or parent anion is not a concern. Finally, while not given explicitly in the tables, G3(MP2) calculations show that the bond enthalpy D_{298}(c-$C_4F_3Cl_2$–F) = 5.10 eV, so that production of F^- ion product in electron attachment to c-$C_4F_4Cl_2$ is endothermic by 1.62 eV. No F^- ion product was expected or observed in these experiments.

The results for c-$C_4F_4Cl_2$ are especially interesting when compared to our previous results on c-$C_6F_8Cl_2$ and c-$C_5F_6Cl_2$, where dissociative electron attachment was also endothermic, but by little enough that Cl^- ion product was observed as the temperature was increased [1,2]. The electron detachment energies for c-$C_6F_8Cl_2^-$ and c-$C_5F_6Cl_2^-$ were too large for them to succumb to thermal electron detachment in our temperature range. The electron attachment rate constant is close to collisional for all three of these molecules, but the end result changes because of small differences in energetics, mainly in EA(c-$C_xF_yCl_2$). For c-$C_6F_8Cl_2$ and c-$C_5F_6Cl_2$, there was a competition between nondissociative and dissociative electron attachment. For c-$C_4F_4Cl_2$ there is only a competition between electron attachment and thermal detachment.

5. Conclusions

Rate constants for electron attachment to c-$C_4F_4Cl_2$ and electron detachment from the parent anion (c-$C_4F_4Cl_2^-$) have been measured over a temperature range from 295 to 556 K in a FALP apparatus. Only the parent anion, c-$C_4F_4Cl_2^-$, was found to result from attachment in this temperature range in a helium buffer gas at 80–160 Pa pressure. Calculations show that there are no exothermic dissociative electron attachment channels for c-$C_4F_4Cl_2$ in the temperature range studied. The electron attachment rate constant was found to be independent of temperature over the range studied, at a value of $(2.4 \pm 0.8) \times 10^{-7}\,cm^3\,s^{-1}$. The rate constant for electron detachment from c-$C_4F_4Cl_2^-$ is strongly temperature dependent, being immeasurable at room temperature but reaching a value of $3100 \pm 1200\,s^{-1}$ at 511 K. The equilibrium constant obtained from these data yields an EA for c-$C_4F_4Cl_2$ of 0.87 ± 0.08 eV. G3(MP2) and density functional calculations were carried out for the c-$C_4F_4Cl_2$ neutral, anion, and fragments in order to aid in interpreting the experiments. The G3(MP2) and DFT calculations yielded EA(c-$C_4F_4Cl_2$) = 0.79 and 0.93 eV, respectively, in good agreement with experiment. The calculations yield structures, atomic charges, dipole moments, heat capacities, and polarizabilities for these molecules. The results for c-$C_4F_4Cl_2$ may be compared to our previous results on c-$C_6F_8Cl_2$ and c-$C_5F_6Cl_2$, where dissociative electron attachment was also endother-

mic, but by little enough that Cl^- ion product was observed as the temperature was increased [1,2]. Further, EA(c-$C_6F_8Cl_2$) and EA(c-$C_5F_6Cl_2$) were calculated to be too large for thermal electron detachment to occur in our temperature range [2].

Acknowledgements

We dedicate this article to Prof. Helmut Schwarz, whose enthusiasm is as inspiring as his work on organic chemistry. We thank the Air Force Office of Scientific Research for its continued support of this laboratory. J.M.V.D. is grateful for support from the Research Corporation, the Camille and Henry Dreyfus Foundation, and the College of the Holy Cross. D.M.K. is grateful for summer support provided by the Howard Hughes Medical Institute. T.M.M. is under contract (F19628-99-C-0069) to Visidyne, Inc., Burlington, MA.

References

[1] J.M. Van Doren, D.M. Kerr, M.D. Hargus, W.M. Foley, S.A. McSweeny, T.M. Miller, R.A. Morris, A.A. Viggiano, W.B. Knighton, Int. J. Mass Spectrom. 195/196 (2000) 517.
[2] T.M. Miller, J.M. Van Doren, A.A. Viggiano, Int. J. Mass Spectrom. 205 (2001) 271.
[3] D. Smith, P. Španěl, Adv. At. Mol. Phys. 32 (1994) 307.
[4] T.M. Miller, A.E.S. Miller, J.F. Paulson, X. Liu, J. Chem. Phys. 100 (1994) 8841.
[5] T.M. Miller, R.A. Morris, A.E.S. Miller, A.A. Viggiano, J.F. Paulson, Int. J. Mass Spectrom. Ion Process. 135 (1994) 195.
[6] T.M. Miller, A.E.S. Miller, A.A. Viggiano, J. Phys. Chem. A 106 (2002) 10200.
[7] Electron–ion recombination depends on the square of the plasma density and thus is unimportant if the plasma density is low enough, especially if n_r is low enough that molecular positive ions are slow to form. Electron–ion recombination depends on, first of all, the production of molecular positive ions by reaction with the plasma Ar^+ and He^+ precursor ions, a relatively slow process, and then on the recombination rate constant. To estimate the contribution of electron–ion recombination, we can assume a collisional rate constant (2×10^{-9} cm^3 s^{-1}) for, say, Ar^+ reacting with c-$C_4F_4Cl_2$, at the concentration used in the example illustrated in Fig. 1, and find that the concentration of molecular positive ions after 1 ms is 10^7 cm^{-3}. Then, we use a typical recombination rate constant of 3×10^{-7} cm^3 s^{-1}, which leads to a recombination frequency (per electron) at 1 ms of 3 s^{-1}, a value which is negligible compared to the electron attachment frequency of 1380 s^{-1} determined from the data in Fig. 1. More complete modeling, taking into account the various coupled charged-particle densities with interaction time, has been reported by T.M. Miller, J.F. Friedman, A.E.S. Miller, J.F. Paulson, Int. J. Mass Spectrom. Ion Process. 149/150 (1995) 111, for a case where the electron attachment rate constant is small enough that n_r is large and recombination loss is important.
[8] A.D. Becke, J. Chem. Phys. 98 (1993) 5648.
[9] L.A. Curtiss, P.C. Redfern, K. Raghavachari, V. Rassolov, J.A. Pople, J. Chem. Phys. 110 (1999) 4703.
[10] M.J. Frisch, G.W. Trucks, H.B. Schlegel, G.E. Scuseria, M.A. Robb, J.R. Cheeseman, V.G. Zakrzewski, J.A. Montgomery Jr., R.E. Stratmann, J.C. Burant, S. Dapprich, J.M. Millam, A.D. Daniels, K.N. Kudin, M.C. Strain, O. Farkas, J. Tomasi, V. Barone, M. Cossi, R. Cammi, B. Mennucci, C. Pomelli, C. Adamo, S. Clifford, J. Ochterski, G.A. Petersson, P.Y. Ayala, Q. Cui, K. Morokuma, D.K. Malick, A.D. Rabuck, K. Raghavachari, J.B. Foresman, J. Cioslowski, J.V. Ortiz, B.B. Stefanov, G. Liu, A. Liashenko, P. Piskorz, I. Komaromi, R. Gomperts, R.L. Martin, D.J. Fox, T. Keith, M.A. Al-Laham, C.Y. Peng, A. Nanayakkara, C. Gonzalez, M. Challacombe, P.M.W. Gill, B. Johnson, W. Chen, M.W. Wong, J.L. Andres, C. Gonzalez, M. Head-Gordon, E.S. Replogle, J.A. Pople, Gaussian 98W, Revision A.7, Gaussian, Inc., Pittsburgh, PA, 1998.
[11] J.P. Perdew, K. Burke, Y. Wang, Phys. Rev. B 54 (1993) 16533;
K. Burke, J.P. Perdew, Y. Wang, in: J.F. Dobson, G. Vignale, M.P. Das (Eds.), Electron Density Functional Theory: Recent Progress and New Directions, Plenum, New York, 1998.
[12] J.C. Rienstra-Kiracofe, G.S. Tschumper, H.F. Schaefer, S. Nandi, G.B. Ellison, Chem. Rev. 102 (2002) 231.
[13] J.B. Foresman, Æleen Frisch, Exploring Chemistry with Electronic Structure Methods, 2nd ed., Gaussian, Inc., Pittsburgh, PA, 1996, p. 64. We used the scaling factor given for B3LYP/6-31G(d) frequencies. We calculated vibrational frequencies for c-$C_5F_6Cl_2$ using both B3LYP/6-31G(d) and B3PW91/6-311+G(d), and found those for the latter to be larger than those for the former by 0.05%, which would affect quantities in Table 1 by less than 1 meV.
[14] M.W. Chase, C.A. Davies, J.R. Downey, D.J. Frurip, R.A. McDonald, A.N. Syverud, JANAF Thermochemical Tables, 3rd ed., J. Phys. Chem. Ref. Data 14 (Suppl. 1) (1986) 718, 720, 1010.
[15] J.B. Foresman, Æleen Frisch, op. cit., pp. 146–158.
[16] U. Berzinsh, M. Gustafsson, D. Hanstorp, A.E. Klinkmueller, U. Ljungblad, A.-M. Maartensson-Pendrill, Phys. Rev. A 51 (1995) 231.
[17] C.E. Klots, Chem. Phys. Lett. 38 (1976) 61.
[18] D. Clary, J.P. Henshaw, Int. J. Mass Spectrom. Ion Process. 80 (1987) 31.
[19] D.H. Williamson, W.B. Knighton, E.P. Grimsrud, Int. J. Mass Spectrom. 195/196 (2000) 481.
[20] A.A. Viggiano, R.A. Morris, F. Dale, J.F. Paulson, K. Giles, D. Smith, T. Su, J. Chem. Phys. 93 (1990) 1149.
[21] A.A. Viggiano, J.F. Paulson, J. Chem. Phys. 79 (1983) 2441.